# Pseudo Continuous Arterial Spin Labeling Quantification in Anemic Subjects with Hyperemic Cerebral Blood Flow

**Adam Bush, Ph.D**[1,2], **Yaqiong Chai, MS**[2], **So Young Choi, MS**[3], **Lena Vaclavu, MS**[4], **Scott Holland, Ph.D**[5], **Aart Nederveen, Ph.D**[4], **Thomas Coates, MD**[6], and **John Wood, MD, Ph.D**[2,7]

[1]Department of Radiology, Stanford University, Palo Alto, California

[2]Department of Biomedical Engineering, University of Southern California, Los Angeles, California

[3]Neurosciences Program, University of Southern California, Los Angeles, California

[4]Department of Radiology, Academic Medical Center, Amsterdam

[5]Department of Radiology, Cincinnati Children's Hospital Medical Center, Cincinnati, Ohio

[6]Division of Hematology, Children's Hospital Los Angeles, Los Angeles, California

[7]Division of Cardiology, Children's Hospital Los Angeles, Los Angeles, California

## Abstract

**Purpose**—To investigate possible sources of quantification errors in global cerebral blood flow (CBF) measurements by comparing pseudo continuous arterial spin labeling (PCASL) and phase contrast (PC) MRI in anemic, hyperemic subjects.

**Methods**—All studies were performed on a Philips 3T Achieva MRI scanner. PC and PCASL CBF examinations were performed in 10 healthy, young adult subjects and 18 young adults with chronic anemia syndromes including sickle cell disease and thalassemia. CBF estimates from single and two compartment ASL kinetic models were compared. Numerical simulation and flow phantom experiments were used to explore the effects of blood velocity and $B1^+$ on CBF quantification and labeling efficiency.

**Results**—PCASL CBF underestimated PC in both populations using a single compartment model ($30.1 \pm 9.2\%$ control, $45.2 \pm 17.2\%$ anemia). Agreement substantially improved using a two-compartment model ($-8.0 \pm 6.0\%$ control, $11.7 \pm 12.3\%$ anemia). Four of the anemic subjects exhibited venous outflow of ASL signal, suggestive of cerebrovascular shunt, possibly confounding PC-PCASL comparisons. Additionally, sub-study experiments demonstrated that $B1^+$ was diminished at the labeling plane ($82.9 \pm 5.1\%$), resulting in suboptimal labeling efficiency. Correcting labeling efficiency for diminished $B1^+$, PCASL slightly overestimated PC CBF in controls ($-15.4 \pm 6.8\%$) and resulted in better matching of CBF estimates in anemic subjects ($0.7 \pm 10.0\%$ without outflow, $10.5 \pm 9.4\%$ with outflow).

Correspondence to: John Wood, MD, PhD, Division of Cardiology, MS #34, Children's Hospital of Los Angeles, 4560 Sunset Blvd, Los Angeles, CA 90027, Tel: 323-361-5470; Fax: 323-361-3668; jwood@chla.usc.

**Conclusions**—This work demonstrates that a two-compartment model is critical for PCASL quantification in hyperemic subjects. Venous outflow and $B1^+$ under-excitation may also contribute to flow underestimation, but further study of these effects is required.

### Keywords

Arterial Spin Labeling; Anemia; Sickle Cell Disease; Labeling Efficiency

## Introduction

Arterial Spin Labeling (ASL) MRI is being used increasingly for quantitative cerebral blood flow imaging due to the ubiquity of MRI scanners, a null contrast requirement, no ionizing radiation exposure, non-invasiveness, excellent patient tolerance and high reproducibility[1,2]. Recently, the ASL consensus document has set guidelines for ASL pulse sequence parameters and post processing strategies[1]. One recommendation of the consensus document was the use of Pseudo Continuous Arterial Spin Labeling (PCASL) because of speed, ease and signal to noise efficiency[3,4]. Additionally, the consensus document recommended the use of a single compartment kinetic tracer model, to convert the measured signal into quantitative units of ml/100g of tissue/minute[5]. Though these recommendations greatly improved the ease, compatibility and robustness of ASL in healthy subjects, their accuracy is incompletely understood in many pathologic conditions.

Chronic anemia is one condition where ASL CBF measurements may require additional optimization. Anemic subjects have elevated CBF[6], high blood velocities[7], shorter vascular transit times[8] and longer blood relaxation times[9,10]. In sickle cell disease (SCD), quantification is complicated further by abnormal blood properties (shorter T1 for a given hematocrit[11]) and cerebrovascular disease (stroke[12,13], vessel tortuosity[14]). As a result, historically there are widely variable reports of ASL CBF values in SCD[8,15–20]. Furthermore, since increased cerebral blood flow and blood velocity are in common young children[21] and subjects undergoing acute hyperemic challenges[22,23], understanding hyperemic ASL quantification errors is critical.

Therefore, to understand the implications of the consensus document recommendations in hyperemic subjects, we compared the CBF values estimated from PCASL with another independent MRI modality, phase contrast (PC). We then used numerical methods to simulate labeling efficiency and a flow phantom to validate those estimates; with the aim to improve ASL quantification in populations with high global CBF.

## Materials and Methods

We performed cerebral MRI in 18 anemic, young adults with and without sickle cell disease (9 SCD and 9 other, non-sickle anemic syndromes) and 10 young adult, healthy control subjects. The average HbS percentage for the SCD subjects was 44.7±19.8%. More demographic information can be found in Table 1. All studies were approved by an institutional review board (CCI-11-00083) and all patients provided informed consent/assent. Subjects were drawn from a larger patient cohort described elsewhere[6,24], but limited to subjects less than 25 years of age to enrich the prevalence of high CBF.

## In Vivo Imaging

A Philips Achieva 3T scanner with an 8 channel receive headcoil and single RF transmission chain was used in all experiments. Cerebral blood flow was measured using both 2D PC and PCASL.

### Phase Contrast

Phase contrast data was presented in a previous study and sequence details can be found therein(6,24). In short, a single 2D axial plane, non-gated phase contrast image was positioned 1-5 cms above the carotid bifurcation. The image slice was positioned to be optimally orthogonal to all four major feeding vessels. The phase contrast sequence parameters included a velocity encoding gradient of 150cm/s, 5 mm slice thickness and 1.08 mm in plane resolution. A semi-automated vessel selection was performed using manual centroid selection and a Canny threshold algorithm(25). Global CBF was calculated as the product of velocity and cross-sectional area using in-house Matlab scripts (Mathworks, Natick, MA).

Phase contrast CBF estimates were stable over time with a coefficient of variation of 4.6 $\pm$ 3.0% over an average of 30.3 $\pm$ 9.5minutes(6). A 3D $T_1$ weighted sequence (1mm$^3$ isotropic resolution) was collected for calculation of total brain volume (Brainsuite.org, v. 15a)(26). A brain density of 1.05g/ml was assumed for conversion of brain volume to brain mass(11,27). For calculation of CBF from phase contrast, total flow through the carotid and vertebral arteries was normalized to the combined mass of the cerebrum, cerebellum, midbrain, pons and brain stem, excluding cerebrospinal fluid.

### Pseudo Continuous Arterial Spin Labeling

A two shot, segmented 3D GRASE, unbalanced PCASL sequence was used for CBF measurements (TR=3800ms, TE 9.8ms, label duration of 2000s and label delay of 1600s). An initial magnetization ($M_0$) image was acquired with identical readout and TR but with an inactive ASL module.

A customized PCASL labeling train included an unbalanced RF pulse train with Hanning shaped RF pulses, maximum gradient amplitude of 10 G/cm and mean gradient of 1 G/cm over the interpulse interval of 1ms with a pulse duration of 0.5ms. Two optimally timed (1616ms, 3150ms), background suppression pulses following labeling were used(28). The inversion efficiency of each background suppression pulse was 95%(29). The imaging plane consisted of ten, 10mm slices, with 3.3mm in plane resolution centered on the corpus callosum. The labeling plane was positioned 90 millimeters inferior of the AC PC line(30). A single, volumetric pencil beam shim was positioned over the image volume and labeling plane. Ten averages were obtained with a total scan time of ~5.5 minutes.

### Cerebral Blood Flow Quantification

Figure 1 depicts a pictorial representation of the two CBF kinetic tracer, quantification models used in this study. First, CBF was quantified using the single compartment model advocated by the ASL consensus document(1), where CBF is calculated as follows:

$$CBF = \frac{6000 * \lambda * (Control - Label) * e^{\frac{PLD}{T_{1b}}}}{2 * LE * T_{1b} * PD * \left(1 - e^{\frac{-\tau}{T_{1b}}}\right)} \ [ml/100g/min]$$

1)

where $\lambda$ is the brain/blood partition coefficient (0.9 ml/g), *PLD* is the post-label delay (1.6 seconds), *PD* is the proton density image intensity, $\tau$ is the PCASL train duration (2.0 seconds) and $T_{1b}$ is the longitudinal relaxation of blood at 3T.

For healthy control subjects and anemic subjects with hemoglobin A, a $T_{1b}$ correction was performed based on each subject's individual hematocrit measurement(9).

$$T_{1b} = \frac{1}{0.52 * HCT + 0.38}$$

2)

Recent work has shown that equation [2] is suboptimal in patients with SCD. Ideally, in vivo patient specific $T_{1b}$ should be measured. When this is unavailable, a population specific $T_{1b}$ of 1818ms should be used instead. For this reason, we used a $T_{1b}$ of 1818ms in all subjects with SCD(11).

### Labeling Efficiency

Labeling efficiency, (LE) is the inversion rate of water protons at the labeling plane and is defined as (control - label)/(2* $M_0$)(31). Global, whole brain LE was determined using numerical simulation and voxelwise cervical phase contrast velocities in the four cerebral feeding vessels. Voxelwise LE estimates were weighted by the velocity based flow contribution.

### Numerical Bloch Simulations

A population of spins moving at a single, constant velocity was modeled as traversing from 1 cm below the labeling plane up until 2 cm above. The model parameters used were chosen similar to arterial human blood including $T_2$= 200ms(10), $T_1$ = 1600ms(9). Numerical simulations were performed on resonance, in the rotating frame with a numerical step size of 3.6 µs. Bloch simulation PCASL parameters matched the ex and in vivo scan, with an unbalanced RF pulse train with Hanning shaped RF pulses, maximum gradient amplitude of 10 G/cm and mean gradient of 1 G/cm over the interpulse interval of 1ms and pulse duration of 0.5ms. Several simulation parameters were iteratively studied including $B1^+$ strength, blood $T_2$ and velocity. Simulations were constructed using in-house Matlab (Mathworks, Natick, MA) scripts.

### Post Hoc Studies Experiments

**Flow Phantom—**A constant pressure, gravity feed, flow phantom was constructed to measure and verify predictions made by numerical simulations (schematic in supplementary materials). The gravity feed system was connected to a 30mm diameter polyvinyl chloride

(PVC) tube. The PVC tube was lined with 3% agarose medium to render variable lumen sizes ranging from 2-10mm and to reduce lumen boundary susceptibility artifacts. To further reduce susceptibility artifacts, the PVC tube was inline and centered in a one liter reservoir (100mm diameter). The reservoir then drained into a downstream receptacle before being pumped back into the gravity feed system. Gadopentate dimeglumine (Magnevist) doped water (0.137 mM, $T_1$ ~1700ms) was used within the circuit to mimic the $T_1$ of blood(32). End resistance of the circuit was modulated to control the flow rate.

Both a 2D phase contrast and modified PCASL sequence was acquired in the phantom to directly compare simulation results to measured estimates of labeling efficiency. A 2D phase contrast sequence with a velocity encoding gradient of 150cm/s, 3mm slice thickness and 0.3 mm in plane resolution was acquired for velocity profile estimates. Averaging over ten dynamics was performed for increased SNR. Semi-automated vessel selection was performed using manual selection and a Canny threshold algorithm. The average, voxelwise velocity data was used in simulations to ascertain a predicted labeling efficiency.

A PCASL labeling efficiency scan was performed, consisting of a fast-readout, line scan sequence which measured the ASL signal in the flowing fluid pool. The scan parameters included a label duration of 500ms, label delay of 10ms and label gap of 1 cm with a multishot, gradient echo readout. PCASL RF train parameters matched in vivo and numerical simulation outlined above. Ten averages were performed for increased SNR. Total scan time was ~6 minutes. Voxelwise, measured labeling efficiency was calculated as (control-label)/(2*control). Additionally, the $B1^+$ was measured across the flow phantom. A dual TR $B1^+$ mapping sequence with inplane resolution of 1mm, slice thickness of 3mm and TE/TR1/TR2=3ms/20ms/120ms was used. Eight, transverse slices, covering the imaging and labeling plane were obtained. Average $B1^+$ of the labeling plane and the adjacent slices was measured throughout agarose medium, excluding the lumen in order to avoid flow related artifacts. $B1^+$ efficiency was defined as the achieved $B1^+$ divided by the designated $B1^+$.

**In Vivo B1 Measurements—**In five separate healthy subjects, whole brain $B1^+$ maps were measured in the sagittal plane using a multislice 2D dual TR $B1^+$ mapping sequence with similar scan parameters as above. Average $B1^+$ was measured at the intersection of the cerebral feeding vessels and the labeling plane.

**Two Compartment Model—**In addition, CBF quantification was performed using a modified two compartment kinetic quantification model proposed by Wang et al(33) (Figure 1):

$$CBF = \frac{6000 * \lambda * (Control - Label) * e^{\frac{\delta}{T_{1b}}}}{2 * LE * T_{1t} * PD * \left(e^{\frac{\delta - PLD}{T_{1t}}} - e^{\frac{\delta - \tau - PLD}{T_{1t}}}\right)} \, [ml/100g/min]$$

$$3)$$

where $\delta$ is the tissue transit time and $T_{1t}$ is the tissue longitudinal relaxation. Voxelwise gray and white matter cerebral perfusion was calculated separately using $T_{1t}$ values of 1332 ms for gray and 850 ms(34) for white matter.

Since we did not measure δ directly, we used literature values to approximate a patient specific δ. Previous reports in healthy subjects have found δ to be approximately 1400ms (35,36). Recently, bolus arrival time (BAT) was measured in patients with SCD and a linear velocity dependence was observed between BAT and average carotid and vertebral velocity, $v_{ave}$(8). Although BAT is systematically shorter than δ, we assumed that BAT would shorten in parallel with increased blood velocity. Using the slope of the BAT-velocity and an assumed δ value of 1400 ms for our healthy subjects ($v_{ave}$=21.5±3.8 cm/s), we derived the following relationship between transit time and mean blood velocities at the labeling plane:

$$\delta = -14.5 * \nu_{ave} + 1710 \quad 4)$$

White matter δ was assumed to be 100ms longer than for gray matter(37).

$T_1$ weighted images were acquired for gray white matter segmentation and processed using BrainSuite (www.brainsuite.org). Gray and white matter probability maps were generated using SPM12 segmentation toolbox(38). The dynamic median of control ASL images were then rigid body registered to the $T_1$ images. Voxelwise gray and white matter probability maps were derived at the same resolution as the ASL images. Sagittal sinus voxels were included in grey and white matter segmentation.

## Results

Across all subjects, the phase contrast measured CBF was 78.6 ± 25.4 ml/100g/min and was tightly correlated with oxygen content, gray white matter ratio and age (previous results) (6,24). Control subjects with the AS (sickle cell trait) and AA genotype exhibited indistinguishable demographics, laboratory values (except mean corpuscular hemoglobin concentration), and cerebral blood flow by PC (64.4 ± 9.5 HbAA and 58.1± 7.7 HbAS, p =0.13) and ASL (75.6 ± 9.9 HbAA and 67.3± 8.1 HbAS p =0.18). Therefore, the two genotypes were combined into a single control group. Population specific values can be found in Table 2. Using a hematocrit corrected, patient specific $T_1$ blood correction and voxelwise flow weighted, labeling efficiency correction, the single compartment ASL quantification model proposed by the consensus document produced an average PCASL CBF of 48.0 ± 9.0 ml/100g/min, demonstrating a relative error of 45.2 ± 17.2%. The relative error between PC and PCASL grew strongly with average flow, $r^2$ = 0.48 (Figure 2, right panels). The discordance between PC and PCASL CBF estimates and the flow related relative error prompted the additional post hoc investigations into error sources.

Representative PCASL single compartment perfusion images can be seen in Figure 2 (left panels). High concentrations of ASL signal appeared in the large cerebral draining veins of four patients (Figure 2, white arrows). Subjects with venous outflow had significantly higher PC CBF and more discordance between PC and single compartment PCASL CBF estimates (Figure 2, filled circles). Additionally, all four patients were more anemic, had high arterial velocities (Table 2) and were receiving chronic transfusion therapy (2 with HbSS SCD and 2 with thalassemia major). Given the quantitative and possible physiologic differences in these patients, for analysis purposes, the results from the venous outflow subjects are reported

both together and separately from the other anemic subjects in Table 2. Separating the venous outflow subjects improved agreement between PC and PCASL CBF measurements in anemic subjects however there remained a statistically significant velocity dependent relative error (Table 2). This residual error prompted the numerical and ex vivo labeling efficiency investigation.

### Numerical Bloch simulation

Numerical simulations of laminar blood flow across the labeling plane produced deterministic results that were in excellent agreement with previous reports in the literature(4,39). Numerical simulations revealed that velocity and $B1^+$ strength were the strongest contributors to diminished labeling efficiency and resultant errors between PCASL and PC CBF measurements. At typical carotid velocities and oxygen saturations, differences in $T_2$ values for healthy and anemic subjects (200ms-300ms) contributed <1.5% to labeling efficiency(10).

Maximal labeling efficiency of 85-90% percent was typically achieved when the blood velocity was in the range of 15-35 cm/s (Figure 3). The relationship between labeling efficiency and velocity was also dependent on the mean $B1^+$. At a mean $B1^+$ of 1.4 uT/ms, the velocity range of optimal labeling efficiency was between 15-35 cm/s. As $B1^+$ decreased, the maximum achievable labeling efficiency decreased and the range of suitable velocities for adequate labeling efficiency narrowed (Figure 3).

### Flow Phantom

In order to verify the Bloch simulations in a controlled environment, we measured labeling efficiency directly in a flow phantom (Figure 4). The phantom maintained a constant, stable and reproducible velocity profile across the vessel lumen (cross section, Figure 4), which allow for exploration of the relationship of velocity and labeling efficiency under steady state conditions. Measured labeling efficiency and predicted labeling efficiency from PC velocity images and numerical simulation were compared on a voxel by voxel basis (Figure 4). Since the imaging phantom was small, transmit gain estimates were inconsistent and we measured a variable $B1^+$ efficiency (80.2%±16.0%) across experimental prescan setup conditions.

Predicted and measured labeling efficiency agreement was highly dependent upon velocity and $B1^+$(Figure 4, bottom panels). Numerical predictions and phantom measurements were in poor agreement when only velocity or the designated $B1^+$ strength was considered alone, especially at high velocity (blue points). By accounting for both the achieved $B1^+$ and velocity, phantom measurements were most similar to numerical model predictions (red points). These results highlighted the interaction between $B1^+$ and blood velocity in determining the labeling efficiency (Figure 4), and suggest that $B1^+$ inhomogeneity could be a significant source of error in subjects with high CBF.

### PCASL B1 correction

Since the contribution of $B1^+$ efficiency to labeling efficiency was discovered post hoc, we could not measure $B1^+$ inhomogeneity in the subjects directly. It is unlikely that chronic

anemia or its other pathologic consequences contribute significantly to $B1^+$ homogeneity in the neck, therefore, we performed $B1^+$ scans in five normal volunteers (4 female, 26.7±4.2 years of age, Figure 5) to assess the potential effect size. The mean $B1^+$ efficiency at the labeling plane was 82.9±5.1% at the intersection of the feeding vessels and the labeling plane compared with a mean $B1^+$ of 105.8%±2.5% in the imaging region (Figure 5). Though the standard deviation of the intersubject $B1^+$ was modest, there was a systematic difference of 12.3 ±6.7% in $B1^+$ between the carotid arteries.

To correct the original PCASL CBF measurements for under-excitation during labeling, we recalculated the patient specific flow weighted labeling efficiency numerically with the population average $B1^+$. Incorporating the influence of measured velocity, hematocrit and $B1^+$ resulted in an average labeling efficiency of 73.9 ± 4.3% across all subjects (population specific Table 2). This resulted in a population CBF of 52.9±11.8 ml/100g/min with a relative error of 36.7 ±15.5% for the single compartment model (Figure 6, leftmost panels). Despite the improvement in agreement in the two techniques, a significant flow dependent relative error remained.

### Two Compartment Model

The two compartment model markedly outperformed the single compartment model in terms of PC and PCASL CBF agreement. Two compartment PCASL CBF across all subjects was 73.4 ± 16.6 ml/100g/min without $B1^+$ correction and 81.0 ± 21.5 ml/100g/min with $B1^+$ correction. The two compartment model lowered the mean and standard deviation of the relative error between PC and PCASL CBF estimates to 4.6 ± 14.3% without $B1^+$ correction and −4.3 ± 12.6% after $B1^+$ correction (Figure 6 middle and right population specific values Table 2). Following $B1^+$ LE correction the PC PCASL relative error was no longer statistically dependent on CBF.

Since equation [3] contains several variables that were not directly measured, we performed sensitivity analysis on some of the key parameters. The 95% confidence intervals of $B1^+$ [72.7% to 93.1%] predicted a mean CBF ranging from 75.1 to 85.9 ml/100g/min, representing a −5.7% to 6.8% difference in CBF. Spatial heterogeneity in $B1^+$ had a potentially large impact on labeling efficiency between the carotid arteries. The average difference in right and left carotid $B1^+$ efficiency (12.3%) would translate to a difference in right-left labeling efficiency (and CBF estimates) of 2.2% at 20 cm/s, 7.0% at 30 cm/s and 11.2% at 40 cm/s.

Additionally, we examined the impact of the uncertainty in transit time. Utilizing published transit time data(35), uncertainty of ±116.7 ms in our population resulted in a 95% confidence interval for mean CBF of 74.8 to 87.8 ml/100g/min, or a relative error of −8.3 ± 1.1% to 7.5 ± 1.0%.

## Discussion

This work identified several important potential confounders of PCASL CBF in estimation including in anemic subjects: use of a single compartment tracer kinetic model, decreased labeling efficiency (from an elevated velocity and $B1^+$ inefficiency) and venous outflow.

## Two Compartment Model

The single largest contributor to PCASL underestimation of PC CBF was the use of a single compartment kinetic tracer model. In the single compartment model, labeled water is assumed to travel intravascularly, from the labeling plane to the imaging voxel, where it instantaneously diffuses from the vessel, homogenously filling the tissue compartment (Figure 1). Given a few reasonable assumptions, ASL is readily quantifiable with the parameters: $\lambda$, $T_{1b}$ and LE. One key assumption is that the longitudinal relaxation values of the intravascular and extravascular space are identical. By assuming equitable relaxation times, the consensus document ASL model neglects the interaction between transit time and tissue $T_1$ values. While this assumption is acceptable for gray matter measurements in healthy subjects ($T_{1b}=1600$ ms and $T_{1t}=1330$ ms)(34) this assumption is less appropriate for white matter ASL quantification ($T_{1t}=850$), and ASL in anemic subjects ($T_{1b} >1800$ ms) (9,11). Shortening of $\delta$ in anemic subjects(8) compounds quantitation errors that arise when identical intravascular and extravascular longitudinal relaxation is assumed. This partially explains why single compartment ASL quantitation errors are largest in anemic, high flow subjects (Figure 2). By using a two compartment model that incorporates a population based estimate of $\delta$ and $T_{1t}$, the velocity dependent disagreement between PCASL and PC was improved, confirming recently published results in SCD patients(8).

## Labeling Efficiency

High blood velocity is common under many physiologic conditions. Blood velocities rise as vessels narrow to enter the skull base and circle of Willis. Additionally, several populations demonstrate higher CBF and/or blood velocity as compared to healthy, adults including school age children, patients with chronic anemia, patients with vessel stenosis and subjects undergoing acute hyperemic challenges (hypercapnia, acetazolamide, etc). Prior numerical empirical work has demonstrated how elevated arterial blood velocity at the labeling plane leads to diminished labeling efficiency because flowing spins receive insufficient excitation pulses required for complete adiabatic inversion(4,15,30). Using a flow phantom and Bloch simulations, we found that increased velocities and $B1^+$ under-excitation synergistically lower labeling efficiency. Although the scanner maximizes $B1^+$ strength allowable under specific absorption rate constraints, we discovered that the $B1^+$ achieved at the labeling plane was approximately 80% of the targeted value. Additionally, the labeling plane is usually several centimeters from isocenter, thus innate, spatial RF carrier wave modulations will result in under excitation in the neck. Both of these phenomena will reduce achieved $B1^+$ and lower labeling efficiency.

Mean blood velocities in the neck in normal subjects are approximately 20-25cm/s. At this velocity and typical $B1^+$ strengths, labeling efficiency remains robust (Figure 3). However, at the blood velocities observed in some anemic subjects, there are greater reductions in labeling efficiency with decreasing achieved $B1^+$ strength (Figure 3). A population based $B1^+$, labeling efficiency correction improved agreement between PC and PCASL CBF estimates, but patient specific $B1^+$ would likely have performed better. Patient specific $B1^+$ measurements could also reduce labeling uncertainties across vascular territories, potentially reducing the reported incidence of left-right ASL perfusion asymmetries in SCD patients(15).

The contribution of $B1^+$ under excitation to labeling efficiency could prove even more problematic for higher field systems because the shorter radiofrequency wavelengths exacerbate $B1^+$ inhomogeneity. In the future, radiofrequency shimming could potentially be used to improve $B1^+$ homogeneity. Alternatively, simultaneous knowledge of $B1^+$ and velocity could provide accurate estimates of labeling efficiency via Bloch simulation. However, these potential solutions need to be prospectively evaluated.

### Venous Outflow

Beside the two compartment model and labeling efficiency, this study identified venous outflow as a possible source of error between PC and PCASL CBF estimates. Phase contrast measures volumetric flow to the brain, regardless of whether the flow is nutritive or non-nutritive, indirectly estimating cerebral perfusion when total brain flow is normalized to brain volume. However, the appearance of labeled blood in the sagittal sinus implies an arteriovenous transit time of <3.6 seconds (sum of label duration and delay), suggesting that a portion of the bolus may have experienced insufficient residence time in capillary beds for normal gas and nutrient exchange (microvascular shunting). Previous groups have observed a similar phenomenon in subjects with known arterio-venous malformations (40) and young, sickle cells patients(41,42) but we demonstrate that the effect is also present in anemic patients with normal hemoglobin. We propose that rapid arterio-venous transit may represent an independent biomarker of disease severity as well as a source of error between ASL and PC CBF estimate but we lacked statistical power to address this possibility.

### Limitations

Although usage of a two compartment model and mean $B1^+$ correction reduced the bias between PC and PCASL CBF values, residual differences remained. One obvious source of variability was the use of population based $\delta$ and $B1^+$ estimates rather than individually measured values. Despite numerous studies, there is little consensus on the most appropriate value to use, with values ranging from close 1 to 2 seconds(8,43). Fortunately, uncertainties in $\delta$ and $B1^+$ efficiency have a much smaller impacted compared to the errors introduce by ignoring $\delta$ or $B1^+$ entirely.

Other sources of error between PC and PCASL CBF include B0 inhomogeneity, uncertainty in $T_{1b}$ values, vessel tortuosity in the labeling plane, unaccounted venous outflow and measurement errors in PC CBF. Off resonance in the labeling plane can result in phase tracking errors which corrupt the adiabatic inversion condition, leading to reduced SNR and labeling efficiency(31,39,44,45). Although correction strategies have been proposed, none have been routinely adopted due to increased scan time and/or difficult implementations(31,39,44,45). In this study, numerical, phantom and in vivo estimates were compared using an assumption of perfect resonance, which is likely untrue in our whole body magnetic system. Unbalanced PCASL will reduce off resonance effects but B0 inhomogeneity remains a limitation of this study and may partially explain the residual relative error and larger variability at higher flow conditions. The interaction of B0 and $B1^+$ is complex(46) and the implications of their simultaneous influence is undescribed in PCASL imaging. Future PCASL studies should focus on the interplay of B0 and $B1^+$ and devise creative solutions that can correct for both inhomogeneities simultaneously.

Another limitation of this study pertains to $T_{1b}$. Recent research has demonstrated that in vivo, patient specific $T_1$ blood measurements improve PCASL quantitation bias and variability(11). In this study, we used a population based blood $T_1$ in our SCD cohort and this may explain some of the residual variability observed. Thirdly, vessel tortuosity at the labeling plane adds an additional path length and angle component to labeling efficiency measurements that was not accounted for in this study. Anemic patients, especially those with sickle cell disease are well known to have tortuous vessels(13) and this fact may partially explain the larger variance observed in the anemic patients in this study. Fourthly, it remains possible that venous outflow is present in other patients but had yet to reach the sagittal sinus at the time of image acquisition. This will also lead to a residual PCASL CBF underestimation and may explain the larger variability in anemic patients.

Lastly, PC is not a gold standard CBF technique for CBF quantitation, thus one cannot wholly attribute systematic differences as errors in PCASL. It is possible that PC is overestimating true CBF due to partial volume, segmentation errors, and vessel obliquity. We chose to use a single measurement plane for all four head vessels to ensure temporal coherence but it is not always possible to position a single plane orthogonal to all four vessels; this is why the ASL measurement plane was a variable distance (2-5 cm) above the carotid bifurcation. We also used a relatively high velocity encoding (150 cm/s) to ensure that no vessels produced any aliasing, even if narrowing or tortuosity was present (our complete study cohort included older subjects). While this lowered the signal to noise ratio, we still had excellent image quality and measurement stability (COV < 5%). Furthermore, our PC CBF measurements had excellent agreement with previously published values measured by Xenon scintography(6,47) and Xenon computed tomography in SCD(48). Greater than 75% of variance in the PC CBF could be explained by inter-patient variations in oxygen content, grey matter volume and patient age, which are all known CBF determinants(6,24). While some studies suggest excellent agreement between PCASL CBF and O-15 $H_2O$ positron emission tomography CBF measurements in normal adults(49,50), comparable studies have not been performed in patients with chronic anemia syndromes.

In conclusion, this is the first study to examine PCASL and PC specifically in high flow conditions including a phantom and in hyperemic patients i.e. adolescents, young adult and patients with sickle cell and other chronic anemia syndromes. PC and PCASL can both be used to for quantitative CBF measurements, however two compartment modeling and $B1^+$ correction should be performed. Contributions from venous outflow must also be considered. Due to the multiple parameters required for accurate PCASL measurements in hyperemic subjects, the authors recommend $B1^+$ mapping and PC CBF estimates accompany quantitative ASL in hyperemic and/or anemic patients to aid estimates of labeling efficiency, anchor global cerebral blood estimates and quantify venous outflow.

## Supplementary Material

Refer to Web version on PubMed Central for supplementary material.

## Acknowledgments

## References

1. Alsop DC, USA BIDMCaHMSDoRBM; Detre JA, USA UoPDoNaRPP; Golay X, UK UIoNDoBRaRL; Günther M, Germany FMB, University Bremen Bremen G, Germany MGH; Hendrikse J, Netherlands UMCUDoRUT; Hernandez-Garcia L, University of Michigan FMRI Laboratory DoBEAAMU; Lu H, USA USMCAIRCDT; MacIntosh BJ, Canada UoTDoMBT, Canada SRIDoPST; Parkes LM, University of Manchester Centre for Imaging Science IoPH, Faculty of Medical and Human Sciences Manchester UK; Smits M, University Medical Centre Rotterdam Department of Radiology EMRTN; Osch MJP, Leiden University Medical Center C. J. Gorter Center for High Field MRI DoRLTN; Wang DJJ, USA UoCLADoNLAC; Wong EC, USA UoCSDDoRaPLJC; Zaharchuk G, USA. SUDoRSC. Recommended implementation of arterial spin-labeled perfusion MRI for clinical applications: A consensus of the ISMRM perfusion study group and the European consortium for ASL in dementia. Magnetic Resonance in Medicine. 2016; 73(1):102–116.

2. Detre JA, Zhang W, Roberts DA, Silva AC, Williams DS, Grandis DJ, Koretsky AP, Leigh JS. Tissue specific perfusion imaging using arterial spin labeling. NMR Biomed. 1994; 7(1–2):75–82. [PubMed: 8068529]

3. Wu WC, Fernandez-Seara M, Detre JA, Wehrli FW, Wang J. A theoretical and experimental investigation of the tagging efficiency of pseudocontinuous arterial spin labeling. Magn Reson Med. 2007; 58(5):1020–1027. [PubMed: 17969096]

4. Dai W, Garcia D, de Bazelaire C, Alsop DC. Continuous Flow Driven Inversion for Arterial Spin Labeling Using Pulsed Radiofrequency and Gradient Fields. Magn Reson Med. 2008; 60(6):1488–1497. [PubMed: 19025913]

5. Buxton RB, Frank LR, Wong EC, Siewert B, Warach S, Edelman RR. A general kinetic model for quantitative perfusion imaging with arterial spin labeling. Magn Reson Med. 1998; 40(3):383–396. [PubMed: 9727941]

6. Borzage MT, Bush AM, Choi S, Nederveen AJ, Vaclavu L, Coates TD, Wood JC. Predictors of cerebral blood flow in patients with and without anemia. J Appl Physiol (1985). 2016; 120(8):976–981. [PubMed: 26796758]

7. Deane CR, Goss D, Bartram J, Pohl KR, Height SE, Sibtain N, Jarosz J, Thein SL, Rees DC. Extracranial internal carotid arterial disease in children with sickle cell anemia. Haematologica. 2010; 95:1287–1292. [PubMed: 20220066]

8. Juttukonda MR, Jordan LC, Gindville MC, Davis LT, Watchmaker JM, Pruthi S, Donahue MJ. Cerebral hemodynamics and pseudo-continuous arterial spin labeling considerations in adults with sickle cell anemia. NMR Biomed. 2017; 30(2)

9. Lu H, Clingman C, Golay X, van Zijl PC. Determining the longitudinal relaxation time (T1) of blood at 3.0 Tesla. Magn Reson Med. 2004; 52(3):679–682. [PubMed: 15334591]

10. Bush A, Borzage M, Detterich J, Kato RM, Meiselman HJ, Coates T, Wood JC. Empirical model of human blood transverse relaxation at 3 T improves MRI T2 oximetry. Magn Reson Med. 2017; 77(6):2364–2371. [PubMed: 27385283]

11. Vaclavu L, van der Land V, Heijtel DF, van Osch MJ, Cnossen MH, Majoie CB, Bush A, Wood JC, Fijnvandraat KJ, Mutsaerts HJ, Nederveen AJ. In Vivo T1 of Blood Measurements in Children with Sickle Cell Disease Improve Cerebral Blood Flow Quantification from Arterial Spin-Labeling MRI. AJNR Am J Neuroradiol. 2016; 37(9):1727–1732. [PubMed: 27231223]

12. Adams RJ, McKie VC, Hsu L, Files B, Vichinsky E, Pegelow C, Abboud M, Gallagher D, Kutlar A, Nichols FT, Bonds DR, Brambilla D. Prevention of a first stroke by transfusions in children with sickle cell anemia and abnormal results on transcranial Doppler ultrasonography. N Engl J Med. 1998; 339(1):5–11. [PubMed: 9647873]

13. Steen RG, Hankins GM, Xiong X, Wang WC, Beil K, Langston JW, Helton KJ. Prospective brain imaging evaluation of children with sickle cell trait: initial observations. Radiology. 2003; 228(1): 208–215. [PubMed: 12759471]

14. Silva GS, Vicari P, Figueiredo MS, Carrete H, Idagawa MH, Massaro AR. Brain magnetic resonance imaging abnormalities in adult patients with sickle cell disease: correlation with transcranial Doppler findings. Stroke. 2009; 40(7):2408–2412. [PubMed: 19443807]

15. Gevers S, Nederveen AJ, Fijnvandraat K, van den Berg SM, van Ooij P, Heijtel DF, Heijboer H, Nederkoorn PJ, Engelen M, van Osch MJ, Majoie CB. Arterial spin labeling measurement of cerebral perfusion in children with sickle cell disease. J Magn Reson Imaging. 2012; 35(4):779–787. [PubMed: 22095695]

16. van den Tweel XW, Nederveen AJ, Majoie CB, van der Lee JH, Wagener-Schimmel L, van Walderveen MA, Poll The BT, Nederkoorn PJ, Heijboer H, Fijnvandraat K. Cerebral blood flow measurement in children with sickle cell disease using continuous arterial spin labeling at 3.0-Tesla MRI. Stroke. 2009; 40(3):795–800. [PubMed: 19150876]

17. Strouse JJ, Cox CS, Melhem ER, Lu H, Kraut MA, Razumovsky A, Yohay K, van Zijl PC, Casella JF. Inverse correlation between cerebral blood flow measured by continuous arterial spin-labeling (CASL) MRI and neurocognitive function in children with sickle cell anemia (SCA). Blood. 2006; 108:379–381. [PubMed: 16537809]

18. Oguz KK, Golay X, Pizzini FB, Freer CA, Winrow N, Ichord R, Casella JF, van Zijl PC, Melhem ER. Sickle cell disease: continuous arterial spin-labeling perfusion MR imaging in children. Radiology. 2003; 227(2):567–574. [PubMed: 12663827]

19. Jordan LC, Gindville MC, Scott AO, Juttukonda MR, Strother MK, Kassim AA, Chen SC, Lu H, Pruthi S, Shyr Y, Donahue MJ. Non-invasive imaging of oxygen extraction fraction in adults with sickle cell anaemia. Brain. 2016; 139(Pt 3):738–750. [PubMed: 26823369]

20. Helton KJ, Paydar A, Glass J, Weirich EM, Hankins J, Li CS, Smeltzer MP, Wang WC, Ware RE, Ogg RJ. Arterial Spin-Labeled Perfusion Combined with Segmentation Techniques to Evaluate Cerebral Blood Flow in White and Gray Matter of Children with Sickle Cell Anemia. Pediatr Blood Cancer. 2009; 52(1):85–91. [PubMed: 18937311]

21. Kety SS. Human cerebral blood flow and oxygen consumption as related to aging. J Chronic Dis. 1956; 3(5):478–486. [PubMed: 13306754]

22. Savourey G, Launay JC, Besnard Y, Guinet A, Travers S. Normo- and hypobaric hypoxia: are there any physiological differences? Eur J Appl Physiol. 2003; 89(2):122–126. [PubMed: 12665974]

23. Vorstrup S, Henriksen L, Paulson OB. Effect of acetazolamide on cerebral blood flow and cerebral metabolic rate for oxygen. J Clin Invest. 1984; 74(5):1634–1639. [PubMed: 6501565]

24. Bush AM, Borzage MT, Choi S, Vaclavu L, Tamrazi B, Nederveen AJ, Coates TD, Wood JC. Determinants of resting cerebral blood flow in sickle cell disease. Am J Hematol. 2016; 91(9): 912–917. [PubMed: 27263497]

25. Kozerke S, Botnar R, Oyre S, Scheidegger MB, Pedersen EM, Boesiger P. Automatic vessel segmentation using active contours in cine phase contrast flow measurements. J Magn Reson Imaging. 1999; 10(1):41–51. [PubMed: 10398976]

26. Shattuck DW, Leahy RM. BrainSuite: an automated cortical surface identification tool. Med Image Anal. 2002; 6(2):129–142. [PubMed: 12045000]

27. Herscovitch P, Raichle ME. What is the correct value for the brain–blood partition coefficient for water? J Cereb Blood Flow Metab. 1985; 5(1):65–69. [PubMed: 3871783]

28. Maleki N, Dai W, Alsop DC. Optimization of background suppression for arterial spin labeling perfusion imaging. Magma. 2012; 25(2):127–133. [PubMed: 22009131]

29. Garcia DM, Duhamel G, Alsop DC. Efficiency of inversion pulses for background suppressed arterial spin labeling. Magn Reson Med. 2005; 54(2):366–372. [PubMed: 16032674]

30. Aslan S, Xu F, Wang PL, Uh J, Yezhuvath US, van Osch M, Lu H. Estimation of labeling efficiency in pseudocontinuous arterial spin labeling. Magn Reson Med. 2010; 63(3):765–771. [PubMed: 20187183]

31. Jahanian H, Noll DC, Hernandez-Garcia L. B0 field inhomogeneity considerations in pseudo-continuous arterial spin labeling (pCASL): effects on tagging efficiency and correction strategy. NMR Biomed. 2011; 24(10):1202–1209. [PubMed: 21387447]

32. Rohrer M, Bauer H, Mintorovitch J, Requardt M, Weinmann HJ. Comparison of magnetic properties of MRI contrast media solutions at different magnetic field strengths. Invest Radiol. 2005; 40(11):715–724. [PubMed: 16230904]

33. Wang J, Alsop DC, Li L, Listerud J, Gonzalez-At JB, Schnall MD, Detre JA. Comparison of quantitative perfusion imaging using arterial spin labeling at 1.5 and 4.0 Tesla. Magn Reson Med. 2002; 48(2):242–254. [PubMed: 12210932]

34. Wansapura JP, Holland SK, Dunn RS, Ball WS Jr. NMR relaxation times in the human brain at 3.0 tesla. J Magn Reson Imaging. 1999; 9(4):531–538. [PubMed: 10232510]

35. Wang J, Alsop DC, Song HK, Maldjian JA, Tang K, Salvucci AE, Detre JA. Arterial transit time imaging with flow encoding arterial spin tagging (FEAST). Magn Reson Med. 2003; 50(3):599–607. [PubMed: 12939768]

36. Chen Y, Wang DJ, Detre JA. Comparison of arterial transit times estimated using arterial spin labeling. Magma. 2012; 25(2):135–144. [PubMed: 21863374]

37. MacIntosh BJ, Filippini N, Chappell MA, Woolrich MW, Mackay CE, Jezzard P. Assessment of arterial arrival times derived from multiple inversion time pulsed arterial spin labeling MRI. Magn Reson Med. 2010; 63(3):641–647. [PubMed: 20146233]

38. Penny, W., Friston, K., Ashburner, J., Kiebel, N. Statistical Parametric Mapping: Analysis of Functional Brain Images. Academic Press; 2006.

39. Zhao L, USA BIDMCaHMSDoRBM; Vidorreta M, USA UoPDoRPP, USA UoPDoNPP; Soman S, USA BIDMCaHMSDoRBM; Detre JA, USA UoPDoRPP, USA UoPDoNPP; Alsop DC, USA BIDMCaHMSDoRBM. Improving the robustness of pseudo-continuous arterial spin labeling to off-resonance and pulsatile flow velocity. Magnetic Resonance in Medicine. 2016

40. Wolf RL, Wang J, Detre JA, Zager EL, Hurst RW. Arteriovenous shunt visualization in arteriovenous malformations with arterial spin-labeling MR imaging. AJNR Am J Neuroradiol. 2008; 29(4):681–687. [PubMed: 18397967]

41. Wu WC, St Lawrence KS, Licht DJ, Wang DJ. Quantification issues in arterial spin labeling perfusion magnetic resonance imaging. Top Magn Reson Imaging. 2010; 21(2):65–73. [PubMed: 21613872]

42. Bush AM, USA SUDoRSC; Coates TD, USA CsHLADoHOLAC; Wood JC, USA CsHLADoCLAC. Diminished cerebral oxygen extraction and metabolic rate in sickle cell disease using T2 relaxation under spin tagging MRI. Magnetic Resonance in Medicine. 2017

43. Liu P, Uh J, Lu H. Determination of spin compartment in arterial spin labeling MRI. Magn Reson Med. 2011; 65(1):120–127. [PubMed: 20740655]

44. Jung Y, Wong EC, Liu TT. Multiphase pseudocontinuous arterial spin labeling (MP-PCASL) for robust quantification of cerebral blood flow. Magn Reson Med. 2010; 64(3):799–810. [PubMed: 20578056]

45. Han PK, Choi SH, Park SH. Investigation of control scans in pseudo-continuous arterial spin labeling (pCASL): Strategies for improving sensitivity and reliability of pCASL. Magn Reson Med. 2016

46. Cunningham CH, Pauly JM, Nayak KS. Saturated double-angle method for rapid B1+ mapping. Magn Reson Med. 2006; 55(6):1326–1333. [PubMed: 16683260]

47. Brown MM, Wade JP, Marshall J. Fundamental importance of arterial oxygen content in the regulation of cerebral blood flow in man. Brain. 1985; 108(Pt 1):81–93. [PubMed: 3978400]

48. Prohovnik I, Pavlakis SG, Piomelli S, Bello J, Mohr JP, Hilal S, De Vivo DC. Cerebral hyperemia, stroke, and transfusion in sickle cell disease. Neurology. 1989; 39(3):344–348. [PubMed: 2927641]

49. Heijtel DF, Mutsaerts HJ, Bakker E, Schober P, Stevens MF, Petersen ET, van Berckel BN, Majoie CB, Booij J, van Osch MJ, Vanbavel E, Boellaard R, Lammertsma AA, Nederveen AJ. Accuracy and precision of pseudo-continuous arterial spin labeling perfusion during baseline and hypercapnia: a head-to-head comparison with (1)(5)O H(2)O positron emission tomography. Neuroimage. 2014; 92:182–192. [PubMed: 24531046]

50. Fan AP, Jahanian H, Holdsworth SJ, Zaharchuk G. Comparison of cerebral blood flow measurement with [15O]-water positron emission tomography and arterial spin labeling magnetic

resonance imaging: A systematic review. J Cereb Blood Flow Metab. 2016; 36(5):842–861. [PubMed: 26945019]
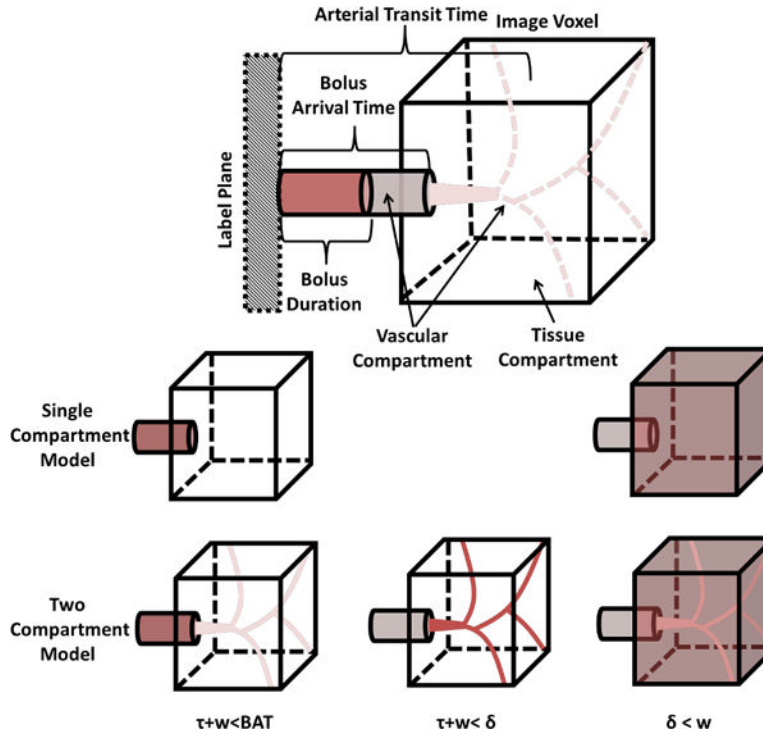
**Figure 1.**
Schematic model of an ASL kinetic compartment model used to convert the measured ASL signal into quantitative cerebral perfusion. In PCASL, a magnetically labeled bolus of blood travels from the labeling plane to the imaging voxel intravascularly. The time at which the bolus arrives at the imaging voxel is defined as the bolus arrival time (BAT). In a single compartment model, perfusion is modeled as the instantaneous diffusion of the bolus into the tissue compartment. In a two compartment model, upon arriving at the imaging voxel the bolus continues intravascularly into the microvascular compartment before diffusing, instantaneously into the tissue compartment. The time it takes the bolus to travel from the labeling plane to the point of microvascular diffusion is termed the arterial transit time, $\delta$. In both models, $\delta$ can be ignored when the longitudinal relaxation of arterial blood and the tissue compartment identical. This assumption is reasonable in the grey matter of healthy subjects, but introduces errors in hyperemic and/or anemic subjects due to faster $\delta$ and longer blood longitudinal relaxation times.
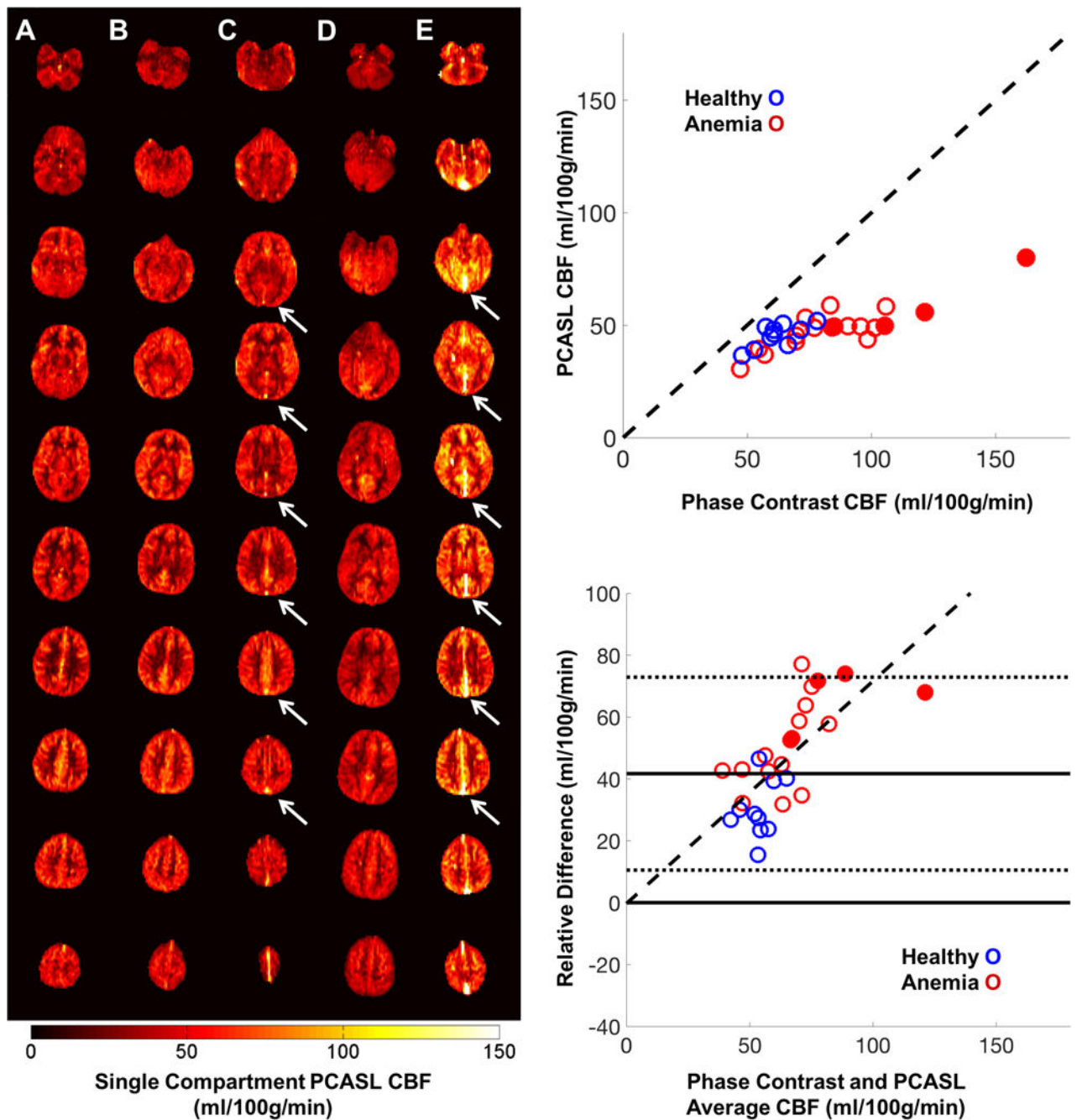
**Figure 2.**
Left) Representative quantitative PCASL CBF maps in 5 subjects (1 CTL [A], 2 anemic, non SCD [B, C] and 2 SCD subjects, [D, E]) with increasing levels of anemia (left to right). Venous ASL signal is present in multiple slices of two anemic subjects (C, E white arrows). Right, Top) PCASL CBF with respect to PC CBF in healthy controls (blue) and anemic subjects (red). Right, Bottom) Bland Altman error plots demonstrate the measurement error grows with flow. Anemic subjects with venous outflow (closed circles) have higher flow and the larger relative error compared to those without venous outflow.
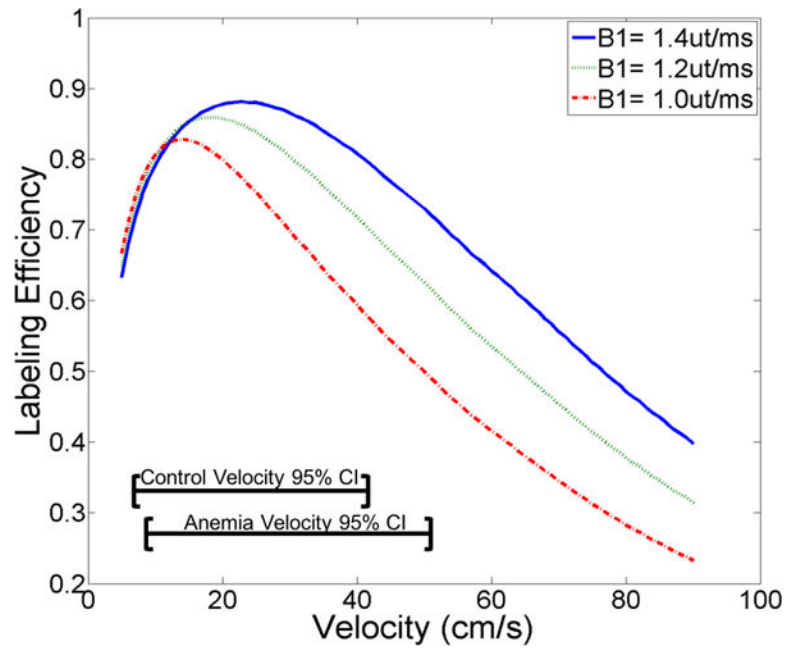
**Figure 3.**
Simulated labeling efficiency as a function of blood velocity for three separate $B1^+$ strengths (textured lines). At lower $B1^+$ values the maximum labeling efficiency drops and the velocity range for optimal labeling narrows.
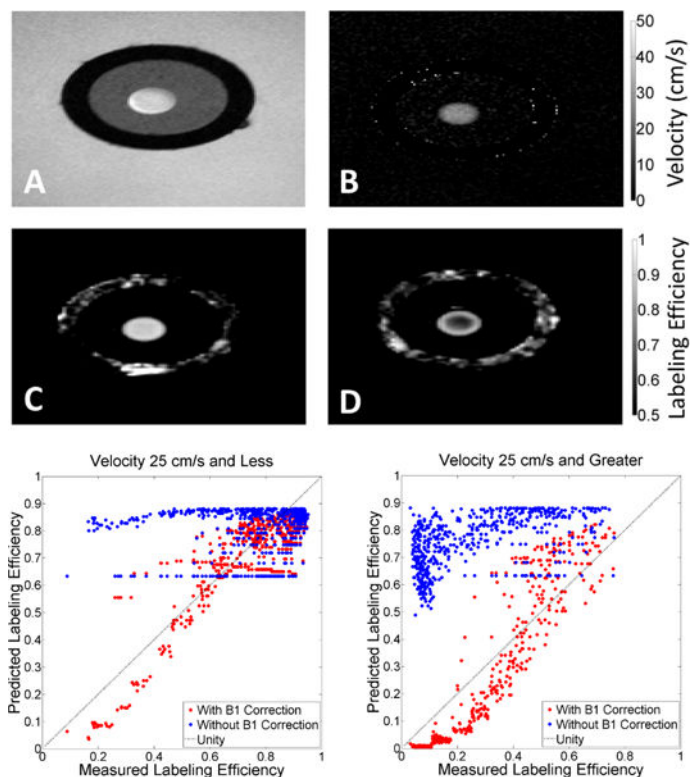
**Figure 4.**

**Top**) Example images acquired from flow phantom used in labeling efficiency validation. A) Phase contrast magnitude image of cross-section of flow phantom. The black ring corresponds to the polyvinyl chloride tube within a water reservoir. The tube was filled with 3% agarose (grey), casting a 2-10mm flow lumen. Constant, steady state, gadolinium doped water flowed through the lumen (white circle) with negligible artifacts. Phase contrast velocity maps (B), along with numerical simulations were used to generate predicted labeling efficiency estimates. C, D) Labeling efficiency maps generated by modified PCASL sequence at two $B1^+$ efficiency values (99% and 65%). At high $B1^+$ efficiency(C), spatial variation of labeling efficiency across the lumen is low. However, higher velocities found in the center of the lumen have noticeably lower labeling efficiency values in low $B1^+$ efficiency conditions (D). **Bottom**) Predicted and measured labeling efficiency was compared for velocities 25 cm/s and >25cm/s. There was poor agreement between predicted and measured labeling efficiency when velocity and designated $B1^+$ was used, especially at high velocity. Agreement between predicted and measured labeling efficiency improved greatly when both velocity and achieved $B1^+$ was incorporated in comparisons of measured and predicted labeling efficiency.
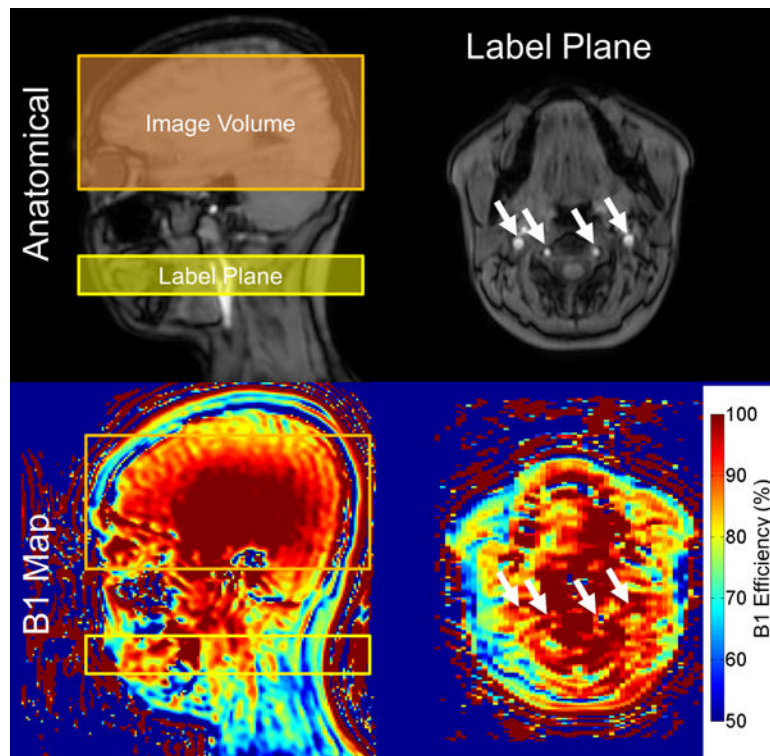
**Figure 5.**
Top) Anatomic sagittal slice demonstrating the localization used in PCASL (left) and a transverse slice of the imaging plane (right). Internal carotid and vertebral arteries are denoted with white arrows. Bottom) Corresponding $B1^+$ maps of the anatomical images. $B1^+$ was significantly diminished at the intersection of the labeling plane and the cerebral feeding vessels compared to the imaging volume. Spatial heterogeneity in $B1^+$ can lead to asymmetries in labeling efficiency that result in perceived asymmetries in CBF.
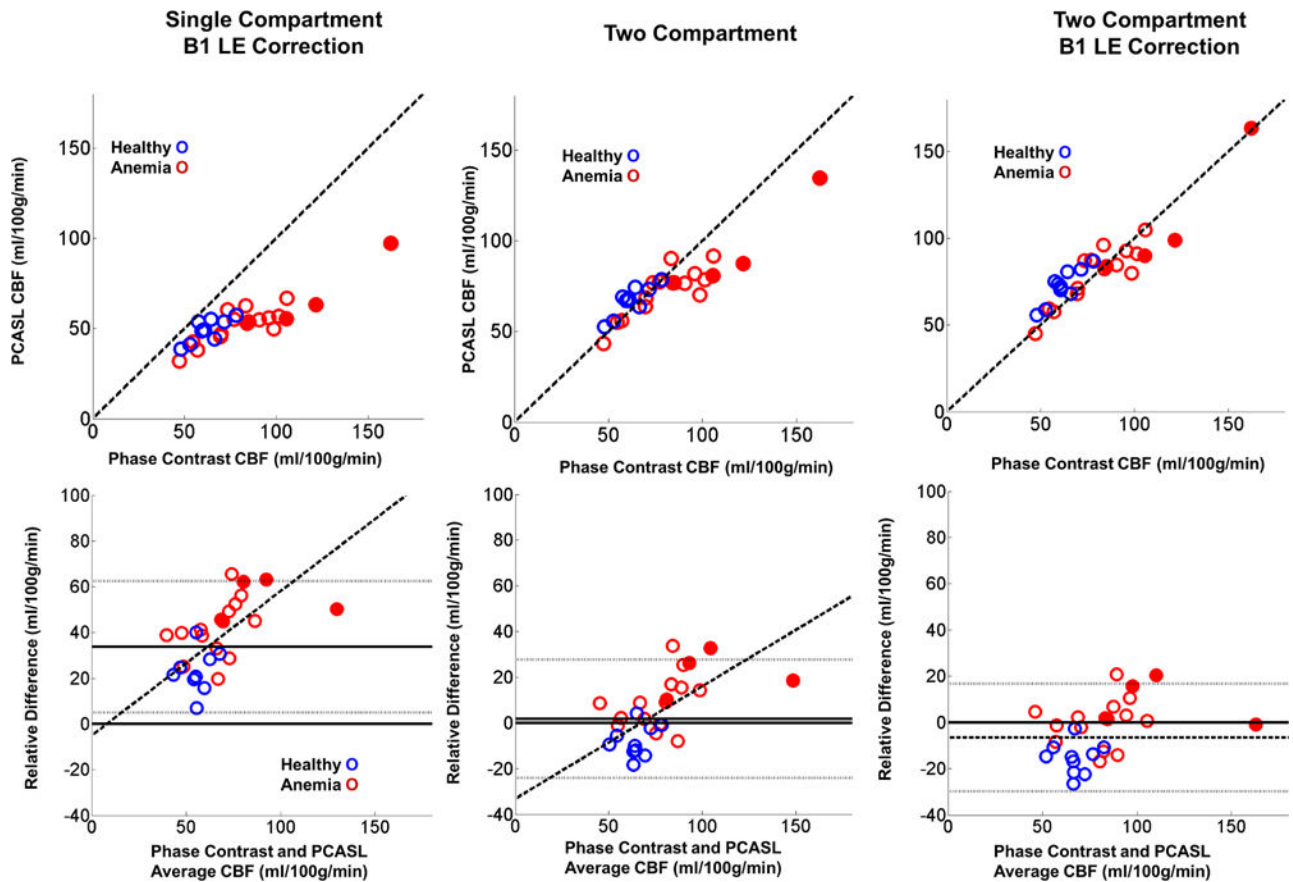
**Figure 6.**

Top) Scatter plot of PCASL and PC CBF using a single compartment model with $B1^+$ adjustment and a two compartment model with and without population $B1^+$ adjustment. Bottom) Corresponding Bland-Altman error plots. The two compartment model greatly removed bias between the two techniques. Following use of a two compartment model with $B1^+$ adjustment, the relative error was no longer flow dependent. Subject specific $B1^+$ estimate would likely further reduce the variance.

**Table 1**

Demographic information.

| | Healthy (Mean ± Std) | Chronic Anemia (Mean ± Std) |
|---|---|---|
| Age (years) | 19.2 ± 4.4 | 18.4 ± 4.4 |
| Sex | 7 Female 3 Male | 9 Female 9 Male |
| Hematocrit (%) | 40.2 ± 4.5 | 31.9 ± 7.4[*] |
| Mean Time Averaged Arterial Velocity (cm/s) | 21.5 ± 3.8 | 25.7± 7.6 |
| Genotype | 6 HbAA 4 HbAS | 3 HbSS, 5 HbSC, HbSF, 4 β thalassemia major, 1 congenital dyserythropoietic anemia, 1 Hemoglobin Eβ thalassemia 0, 2 hereditary spherocytosis, 1 autoimmune hemolytic anemia. |
| Self Reported Racial/Ethnic Background | 8 Black 1 Hispanic, 1 Middle Eastern | 5 Asian, 7 Black, 5 Hispanic, 1 Middle Eastern |

[*] values are statistically different between populations using student t test (p 0.05)

**Table 2**

Cerebral blood flow parameters for separate study populations.

| | Healthy (Mean ± Std) | Chronic Anemia (Mean ± Std) | Chronic Anemia without venous outflow (Mean ± Std) | Anemic Subjects with Venous Outflow (Mean ± Std) |
|---|---|---|---|---|
| PCASL CBF (ml/100g/min) | 45.5 ± 5.1 | 49.4 ± 10.1 | 46.8 ± 7.1 | 58.8 ± 14.4 |
| Relative Error PC-PCASL CBF (%) | 30.1 ± 9.2 | 53.6 ± 13.8 | 49.5 ± 13.8 | 68.1 ± 6.7 [*] |
| PCASL CBF B1 (ml/100g/min) | 49.1 ± 6.1 | 55.0 ± 13.8 | 51.4 ± 7.1 | 67.7 ± 20.1 |
| Relative Error PC-PCASL CBF B1 (%) | 22.8 ± 8.9 | 44.5 ± 12.9 | 41.5 ± 12.2 | 56.1 ± 7.4 [*,+] |
| PCASL CBF (ml/100g/min) | 66.8 ± 7.3 | 75.2 ± 16.4 | 71.1 ± 12.4 | 89.5 ± 20.9 |
| Relative Error PC-PCASL CBF (%) | −7.8 ± 7.2 | 13.5 ± 14.3 [*] | 9.1 ± 14.3 [*] | 28.5 ± 8.0 [*,+] |
| PCASL CBF ATT (ml/100g/min) | 67.0 ± 7.9 | 77.0 ± 19.1 | 71.9 ± 13.6 | 94.8 ± 26.9 |
| Relative Error PC-PCASL ATT CBF (%) | −8.1 ± 6.8 | 11.6± 11.4 [*] | 12.3 ± 11.4 [*] | 23.6 ± 7.3 [*,+] |
| PCASL CBF B1 (ml/100g/min) | 72.3± 9.8 | 85.5 ± 24.9 [*] | 79.1 ± 16.8 | 109.3 ± 36.3 |
| Relative Error PC-PCASL Two Compartment CBF B1 (%) | −15.4 ± 6.8 | 1.8 ± 10.7 [*] | −0.7 ± 10.0 [*] | 10.5 ± 9.4 [*,+] |
| Velocity Corrected Labeling Efficiency | 81.3 ± 1.0 | 80.6 ± 3.1 | 81.0 ± 2.0 | 79.3 ± =−5.8 |
| Velocity and B1 Corrected Labeling Efficiency | 75.5 ± 2.1 | 73.1 ± 5.1 | 74.1 ± 4.0 | 69.8 ± 7.6 |

[*] values are statistically different that the control population using Dunnett's test($p$ 0.05),

[+] values are statistically different than the non venous outflow, anemic subjects using student t statistic($p$ 0.05)